Radiation Pressure Vortices in Two Crossed Standing Waves

A. Hemmerich and T. W. Hänsch
Sektion Physik der Universität München, Schellingstrasse 4/III, D-8000 München 40, Germany and Max-Planck-Institut für Quantenoptik, D-8046 Garching, Germany
(Received 26 December 1991)

We have observed the effect of microscopic radiation pressure vortices on atomic motion in two crossed, near-resonant, optical standing waves. When the two standing waves oscillate synchronously the resulting light field and the corresponding light forces possess a 90° rotation symmetry. However, when one of the standing waves' oscillations is delayed with respect to those of the other, a vortical radiation pressure force arises which can be identified by the breaking of this symmetry. Radiation pressure vortices should play a significant role for the atomic kinematics in optical molasses and magneto-optical traps.

PACS numbers: 32.80.Pj

Neutral atoms can experience strong friction forces when traveling in a near-resonant optical standing wave. In the intersection region of three mutually orthogonal optical standing waves the atoms behave as if moving in a strongly viscous medium [1]. Extremely cold samples of neutral atoms have been prepared in such "optical molasses" [2]. The present one-dimensional theory has been quite successful at explaining many of the features of optical molasses [3]. However, various unexplained experimental observations [4–6] suggest that the physics of light forces in two or three dimensions gives rise to phenomena which cannot be accounted for in a one-dimensional model.

In this Letter we report on the first observation of the effect of microscopic radiation pressure vortices (RPV) on atomic motion. These RPV's constitute a significant example of an inherently multidimensional phenomenon. More precisely, our subject is a radiation pressure field which possesses closed paths on the submicron scale along which the force has tangential direction everywhere. The strength of this vortical radiation pressure is comparable to that of the radiation pressure in an ordinary traveling wave. A first theoretical indication of the existence of vortex forces has been given by Kazantsev and Krasnov [7]. We believe that the study of RPV's provides an important step towards a better understanding of the action of light forces in two and three dimensions. To study a particularly simple example of RPV's, we have investigated the kinematics of rubidium atoms in a two-dimensional light field. The significance of RPV's in the more complex three-dimensional case of optical molasses will be an interesting subject of further research.

Let us start with a brief review of the light forces expected to act on a neutral atom resting at the position $\mathbf{r}_0$ in an arbitrary radiation field. On the one hand, the induced oscillating electric dipole moment $\mathbf{P}$ of the atom gives rise to a time-averaged Lorentz force

$$\mathbf{F}_L=\left\langle\frac{\partial}{\partial t}\mathbf{P}\times\mathbf{B}\right\rangle=-\left\langle\mathbf{P}\times\frac{\partial}{\partial t}\mathbf{B}\right\rangle=\langle\mathbf{P}\times(\nabla\times\mathbf{E})\rangle. \quad (1)$$

Here and in the following, the brackets $\langle\,\rangle$ denote the time average. On the other hand, the Coulomb force acting on the atom's rapidly oscillating valence electron [with position $\mathbf{r}(t)=\mathbf{r}_0+e^{-1}\mathbf{P}(\mathbf{r}_0,t)$] can give rise to a nonvanishing time-averaged force term

$$\mathbf{F}_C=\langle e\mathbf{E}(r(t),t)\rangle=\langle(\mathbf{P}\nabla)\mathbf{E}\rangle. \quad (2)$$

The total force is the sum of these two forces, i.e.,

$$\mathbf{F}=\mathbf{F}_L+\mathbf{F}_C=\langle\nabla_E(\mathbf{PE})\rangle, \quad (3)$$

where the index E on the nabla operator ∇ restricts its action to the spatial variables of $\mathbf{E}$.

Now assume the electric field is harmonic, i.e., $\mathbf{E}(r,t)=\mathbf{E}(r)e^{i\omega t}+\mathbf{E}^*(r)e^{-i\omega t}$, and hence $\mathbf{P}(r,t)=\mathbf{P}(r)e^{i\omega t}+\mathbf{P}^*(r)e^{-i\omega t}$. Inserting these expressions into Eq. (3) the total force reads $\mathbf{F}=\nabla_E(\mathbf{PE}^*)+\nabla_E(\mathbf{EP}^*)$. We express $\mathbf{P}$ by the polarizability tensor α, i.e., $\mathbf{P}=\alpha(\mathbf{E})\mathbf{E}$ and assume the tensor α to be complex to account for dissipation. If we work in a suitable basis the tensor α is diagonal with the diagonal elements $\alpha_{\nu\nu}=\alpha_\nu+i\beta_\nu$ expressed in terms of their real and imaginary parts. If we in addition express the components $\mathbf{E}_\nu$ of the complex electric field $\mathbf{E}$ in this basis as $\mathbf{E}_\nu=I_\nu^{1/2}\exp(i\psi_\nu)$ we obtain the total force as

$$\mathbf{F}=\sum_{\nu=1}^{3}\alpha_\nu\nabla I_\nu+2\sum_{\nu=1}^{3}\beta_\nu I_\nu\nabla\psi_\nu. \quad (4)$$

In this expression the total force is a sum of a dipole force (left term) and a radiation pressure force (right term).

In our experiment we employ the particularly simple configuration of two crossed one-dimensional optical standing waves oriented along the x and y axis, respectively. Both are linearly polarized along the z axis and have the same frequency. In this case the Coulomb force vanishes leaving us only with a Lorentz force. However, it should be noted that the phenomena discussed here occur in any 2D and 3D configuration produced by intersecting one-dimensional standing waves which provide interfering polarization components. Our light field is just the simplest example; a more complex example is the $\sigma^+\sigma^-$ polarization scheme used in optical molasses and magneto-optical traps. We may write our light field as $\mathbf{E}=\hat{\mathbf{z}}I^{1/2}\exp(i\psi)$ with time-averaged electric energy density I, local phase ψ, and constant linear polarization

along the z axis. Assuming a scalar polarizability for the atoms, i.e., $\alpha_v=\alpha$ and $\beta_v=\beta$, we arrive at the expression

$$\mathbf{F}=\alpha\nabla I+2\beta I\nabla\psi\,, \tag{5}$$

which is known from two-level atom theory. The polarizability components α and β are obtained by solving the optical Bloch equation for two-level atoms [8]. In our light field the expression $I\nabla\psi$ coincides (up to a constant) with the Poynting vector and has the explicit form

$$I\nabla\psi=\nabla\times[I_0 k\sin(\phi)\sin(kx)\sin(ky)\hat{\mathbf{z}}]\,,$$
$$I=I_0[\cos^2(kx)+\cos^2(ky)+2\cos(\phi)\cos(kx)\cos(ky)]\,, \tag{6}$$

where ϕ denotes the time-phase difference between the two one-dimensional standing waves, k is the wave number, and $\hat{\mathbf{z}}$ denotes the unit vector in the z direction. As is seen from Eq. (6), for $\phi\neq 0°$ our light field acquires some local traveling-wave character, manifesting itself in a nonvanishing electromagnetic energy flow $I\nabla\psi$ which can be expressed as a curl of a vector potential and consists of a square array of submicron vortices. As illustrated in Fig. 1 these vortices have a diameter of half a wavelength. From the second term of Eq. (5) we expect a corresponding field of radiation pressure vortices.

In the following discussion we assume that a collimated beam of neutral atoms is injected into the 2D field along the z axis and we ask how the RPV's can be detected by observing the deflection of the atomic beam. Note that the set of locations where four vortices meet can be subdivided into two classes. Let us specify that energy flows towards class A points along the x axis and away from such points along the y axis and vice versa for class B points. The geometry of the Poynting field at the two locations reminds us of a quadrupole field. A 90° rotation around an A or B point is not a symmetry transformation of the Pynting field as it maps class A onto class B points. This characteristic property carries over to the corresponding radiation pressure field and thus offers the possibility of identifying it experimentally. Note, however, that a combination of a 90° rotation with a $\lambda/2$ translation along the x or y axis remains a symmetry transformation. At first glance, this might lead to the incorrect conclusion that the action of the RPV's on a macroscopic scale (e.g., the deformation of the atomic beam) should remain invariant under 90° rotations with respect to the z axis.

To break the 90° rotation symmetry on a macroscopic scale we take advantage of the dipole forces arising from the first term in Eq. (5). Away from exact resonance these forces act to channel the atoms in the energy density interference pattern I of the light field [given in the second line of Eq. (6)] yielding a dipole force proportional to the gradient of I. Channeling in the 2D field employed here has been extensively discussed in Ref. [9]. Recall that positive (negative) detuning of the light frequency with respect to the atomic resonance yields channeling in the nodes (antinodes) of the light field. For $\phi\neq 90°$ we may choose whether we want the atoms to be predominantly channeled to either class A points or class B points, because the energy density then differs at the two classes of locations. For example, consider the situation arising for $\phi=45°$ which is illustrated in Fig. 2. At blue detuning the atoms are channeled in the vicinity of class B (center of Fig. 2) rather than class A points because B points exhibit lower energy density. Thus, most atoms experience a dipole force which is directed towards the B points and a radiation pressure force field which approximately has a quadrupole geometry with respect to

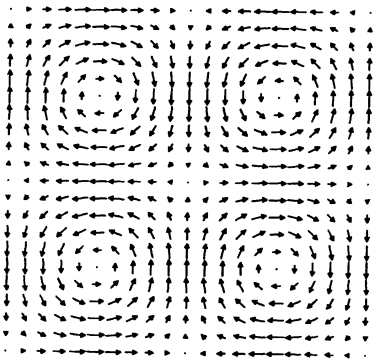

FIG. 1. The flow of electromagnetic energy in the intersection region of two crossed standing waves as given by Eq. (1) at $\phi=90°$. The section shown has a width of one optical wavelength.

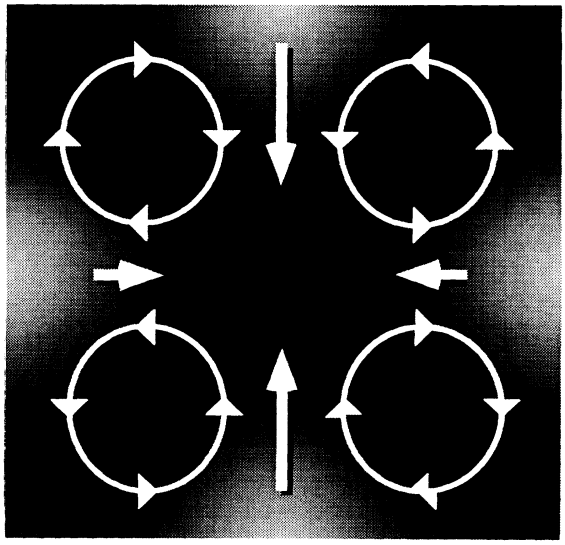

FIG. 2. Location of the energy flow vortices (circles) with respect to the energy density distribution at $\phi=45°$ (background structure). The arrows attached to the circles indicate the sense of rotation of the vortices. The additional vertical and horizontal arrows illustrate the total force. Dark regions of the background structure indicate low energy density. The same section is shown as in Fig. 1.

the B points. As a result, the y component of the total force on average is larger than its x component. This results in an elliptic transverse shape of the atomic beam with eccentricity along the y axis. In the consideration above, A and B class points are interchanged by a sign flip either of $\sin(\phi)\cos(\phi)$ or of the detuning δ, and we thus expect the ellipse to be rotated by 90° in both cases (e.g., when $\phi=135°$). A sign switch of $\sin(\phi)$ interchanges the locations of A and B points because it yields a reversed sense of rotation of the RPV's. A switch of the sign of $\cos(\phi)$ is equivalent to a translation of the energy density pattern by half a wavelength, resulting in a commutation of the node and antinode locations.

Let us summarize our considerations by means of symmetry arguments. Unless ϕ is equal to $0° \pm n\,90°$, where n is an integer, the total force field (i.e., the radiation pressure and the dipole force taken together) is no longer invariant under a combination of a 90° rotation with a $\lambda/2$ translation. The radiation pressure force by itself contributes a lack of 90° rotation invariance whereas the dipole force adds in a lack of $\lambda/2$ translation invariance. The observation of an elliptic transverse density distribution of the atomic beam is a clear indication of the action of vortical radiation pressure.

In our experiment a collimated (0.23 mrad) thermal (300 °C) rubidium beam traversed the optical field of two crossed standing waves produced by splitting the collimated output from an optically stabilized diode laser and retroreflecting both light beams with dielectric planar mirrors. The laser beam diameter was 6 mm, yielding a transit time of 16 μs (i.e., 500 lifetimes of the excited state) for atoms with the most probable velocity of 380 m/s. Only 1.2 mW of the 15-mW laser output was used, in order to achieve an antinode Rabi frequency of two natural linewidths in each of the standing waves. The laser had a spectral linewidth of less than 20 kHz and operated in the neighborhood of the $F=3 \rightarrow F=4$ hyperfine line of the D_2 transition of rubidium 85. The time-phase difference ϕ was controlled by adjusting the optical path length difference between the laser and the two retroreflecting mirrors. In the interaction zone the atomic beam had a diameter of 50 μm. The atomic density distribution was spatially resolved in two dimensions 32 cm downstream from the interaction zone. To achieve this, the atoms traversed a thin (20 μm) sheet of light resonant with the D_1 line which also originated from a diode laser. The fluorescence was monitored by means of a multichannel-plate image intensifier and a charge-coupled-device camera [10]. In order to prepare a closed-cycle system a third diode laser with 20-MHz bandwidth operating at the $F=2 \rightarrow F=3$ hyperfine transition illuminated the interaction region with an intensity of about 1 mW/cm^2. This laser served to counteract optical pumping into the $F=2$ ground state. As a frequency reference for each laser we employed separate saturation spectroscopy setups with rubidium vapor cells.

In Fig. 3(a) we have recorded the transverse profile of the atomic beam after the interaction when the frequency of the standing wave was positively (blue) detuned by two linewidths (i.e., $\delta/\Gamma=2$) with respect to the $F=3 \rightarrow F=4$ hyperfine line. The time-phase difference ϕ was varied clockwise in steps of 45° starting at 0° in the upper right corner. As predicted, the atomic beam acquires an elliptic shape at phase angles 45° and 135°. When we approach zero detuning for $\phi=90°$, the atoms are deflected mainly along the diagonals, as is apparent in the lower left detail of Fig. 3(a). This reflects the following interesting property of the RPV's. Halfway between

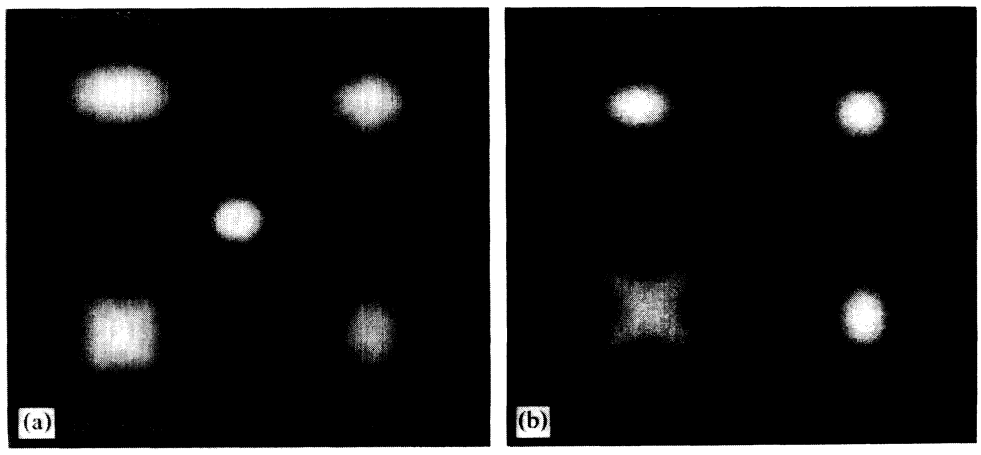

FIG. 3. (a) Atomic beam profiles observed for various values of the time-phase difference ϕ at positive detuning $\delta/\Gamma=2$. The antinode Rabi frequency per standing wave was 2Γ. The standing wave axes are oriented along the vertical (y) and horizontal (x) directions. The feature in the center of the figure is 130 μm in diameter and shows the atomic beam when both standing waves were disabled. For atoms with the most probable longitudinal velocity of 380 m/s, a distance of 100 μm corresponds to a deflection introduced by 20 photon recoils. The pictures were taken 350 mm downstream from the interaction zone. (b) Model calculations corresponding to (a).

two diagonal [i.e., (1,1) or (−1,1)] lattice lines of the vortex lattice shown in Fig. 1 there is always a line along which the radiation pressure force does not alternate in direction. Along these trajectories the atoms are accelerated very efficiently. Such a behavior cannot be explained by elastic scattering from the $\phi=90°$ trap potential [10]. The detail in the center of Fig. 3(a) shows the atomic beam when both standing waves are disabled. When we adjusted for negative (red) detuning the orientations of the ellipses at $\phi=45°$ and $\phi=135°$ were interchanged; for $\phi=0°$ and $\phi=90°$ we observed similar patterns as in the corresponding cases in Fig. 3(a), although with slightly less contrast.

As a theoretical check of our observations, we have programmed a computer simulation of our experiment. This calculation treats the atoms as classical particles which are scattered by a classical force field. Since the transverse velocities of the atoms are much smaller than Γ/k we calculated the force by inserting polarizability components α and β into Eq. (5) as derived from a steady-state solution of a two-level optical Bloch equation [8]. No momentum diffusion [8] mechanism has been built into our program. The results for the same set of parameters as in Fig. 3(a) are presented in Fig. 3(b), showing that such a simple model can basically account for the experimental observations.

In summary, we have studied the role of radiation pressure vortices for the kinematics of rubidium atoms in two crossed linearly polarized optical standing waves. Radiation pressure vortices are present in most other two- or three-dimensional configurations, in particular in the $\sigma^+\sigma^-$ polarization scheme which is employed in optical molasses or magneto-optical traps. Our experiment indicates that vortex forces might also have significant influence on the atomic kinematics in those cases. For example, in experiments with optical molasses vortex forces should lead to a considerable heating effect. In particular, a misalignment of the molasses beams causes a variation of the time-phase differences across the molasses region. In regions where the time-phase differences are not zero one obtains a nonvanishing vortex force which is likely to expel the atoms towards regions where the vortex force vanishes. Thus, one expects to observe macroscopic dark striations in misaligned molasses as has been reported recently [5].

We acknowledge discussions with T. Esslinger and E. Arimondo. This work has been supported in part by the Deutsche Forschungsgemeinschaft.

[1] S. Chu, L. Hollberg, J. Bjorkholm, A. Cable, and A. Ashkin, Phys. Rev. Lett. **55**, 48 (1985).

[2] P. Lett, R. Watts, C. Westbrook, and W. Phillips, Phys. Rev. Lett. **61**, 169 (1988).

[3] J. Dalibard and C. Cohen-Tannoudji, J. Opt. Soc. Am. B **6**, 2023 (1989).

[4] S. Chu, M. G. Prentiss, A. E. Cable, and J. E. Bjorkholm, in *Laser Spectroscopy VIII*, edited by W. Persson and S. Svanberg (Springer-Verlag, Berlin, 1987), p. 58.

[5] N. P. Bigelow and M. G. Prentiss, Phys. Rev. Lett. **65**, 29 (1990).

[6] B. Sheehy, S. Shang, R. Watts, S. Hatamian, and H. Metcalf, J. Opt. Soc. Am. B **6**, 2165 (1989).

[7] A. P. Kazantsev and I. V. Krasnov, J. Opt. Soc. Am. B **6**, 2140 (1989).

[8] J. P. Gordon and A. Ashkin, Phys. Rev. A **21**, 1606 (1980).

[9] A. Hemmerich, D. Schropp, and T. W. Hänsch, Phys. Rev. A **44**, 1910 (1991).

[10] A. Hemmerich, D. Schropp, T. Esslinger, and T. W. Hänsch, Europhys. Lett. (to be published).

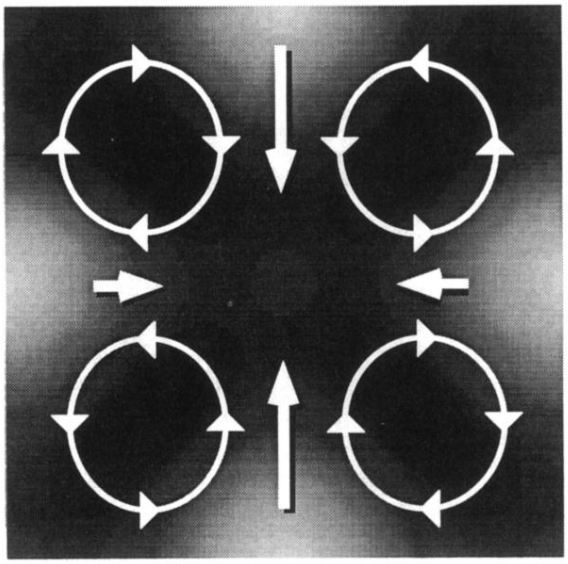

FIG. 2. Location of the energy flow vortices (circles) with respect to the energy density distribution at $\phi=45°$ (background structure). The arrows attached to the circles indicate the sense of rotation of the vortices. The additional vertical and horizontal arrows illustrate the total force. Dark regions of the background structure indicate low energy density. The same section is shown as in Fig. 1.

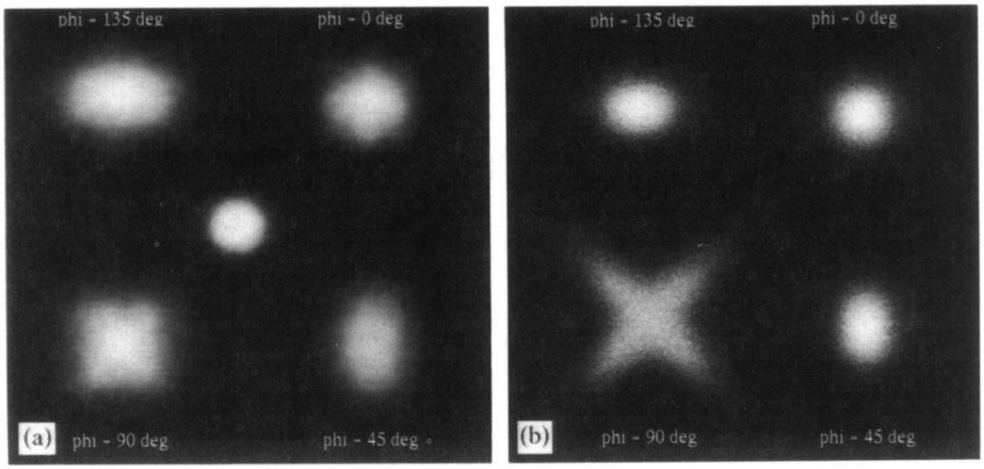

FIG. 3. (a) Atomic beam profiles observed for various values of the time-phase difference ϕ at positive detuning $\delta/\Gamma = 2$. The antinode Rabi frequency per standing wave was 2Γ. The standing wave axes are oriented along the vertical (y) and horizontal (x) directions. The feature in the center of the figure is 130 μm in diameter and shows the atomic beam when both standing waves were disabled. For atoms with the most probable longitudinal velocity of 380 m/s, a distance of 100 μm corresponds to a deflection introduced by 20 photon recoils. The pictures were taken 350 mm downstream from the interaction zone. (b) Model calculations corresponding to (a).